REPORT DOCUMENTATION PAGE

Form Approved
OMB No. 0704-0188

PLEASE DO NOT RETURN YOUR FORM TO THE ABOVE ORGANIZATION.

1. REPORT DATE *(DD-MM-YYYY)*	2. REPORT TYPE	3. DATES COVERED *(From - To)*
30/03/2006	Final Technical	1/1/2003 - 31/12/2005

4. TITLE AND SUBTITLE
Size-selected cluster deposition, applied to monopropellant catalysts.

5a. CONTRACT NUMBER

5b. GRANT NUMBER
F49620-03-1-0062

5c. PROGRAM ELEMENT NUMBER

6. AUTHOR(S)
Scott L. Anderson

5d. PROJECT NUMBER

5e. TASK NUMBER

5f. WORK UNIT NUMBER

7. PERFORMING ORGANIZATION NAME(S) AND ADDRESS(ES)
Chemistry Dept., University of Utah
315 S. 1400 E. Rm 2020
Salt Lake City, UT 84112

8. PERFORMING ORGANIZATION REPORT NUMBER

9. SPONSORING/MONITORING AGENCY NAME(S) AND ADDRESS(ES)
Air Force Office of Scientific Research
875 Randolph St
Suite 325, Rm 3112
Arlington, VA 22203
Dr Michael Berman

10. SPONSOR/MONITOR'S ACRONYM(S)
AFOSR/ NL

11. SPONSOR/MONITOR'S REPORT NUMBER(S)
AFRL-SR-AR-TR-06-0103

12. DISTRIBUTION/AVAILABILITY STATEMENT
unlimited ~Distribution A

13. SUPPLEMENTARY NOTES

14. ABSTRACT
Size-selected cluster deposition was used to prepare model Ir/alumina catalysts, and hydrazine decomposition over such catalysts was studied. Strong effects of both cluster size and alumina preparation conditions were observed. A novel pulsed, inert, ultra-high vacuum-compatible hydrazine inlet system is described

15. SUBJECT TERMS
hydrazine, catalyst, monopropellant, iridium, alumina

16. SECURITY CLASSIFICATION OF:			17. LIMITATION OF ABSTRACT	18. NUMBER OF PAGES	19a. NAME OF RESPONSIBLE PERSON
a. REPORT	b. ABSTRACT	c. THIS PAGE			Scott L. Anderson
none	none	none	none	14	19b. TELEPHONE NUMBER *(Include area code)* (801) 585-7289

Executive Summary

Accomplishments in several areas are described: Integration of a new ultrahigh vacuum (UHV) endstation into the Utah cluster deposition instrument. Development of a hydrazine and UHV-compatible pulsed inlet system. A study of the physical, electronic, and chemical properties of Ir clusters deposited on rutile TiO_2(110), including thermal stability of the Ir/TiO_2 system. A study of hydrazine decomposition on a model high coverage Ir/Al_2O_3/NiAl(110) catalyst over the temperature range from ~120 to 800K. A study of pulsed hydrazine decomposition on the model high coverage catalyst at 400 - 600 K. A study of hydrazine decomposition in temperature-programmed desorption from size-selected Ir_n ($n \leq 15$) on Al_2O_3/NiAl(110), showing strong size effects in both activity and product distributions. A study of Ir-catalyzed aluminum nitride formation in hydrazine exposures to alumina, and passivation of alumina films by hydrazine exposures. A study of hydrazine decomposition in temperature-programmed desorption from size-selected Ir_n ($n \leq 15$) on *passivated* Al_2O_3/NiAl(110), showing strong size effects in both activity and product distributions, and significant differences compared to the unpassivated alumina surface.

Personnel supported:

PI: Scott L. Anderson
Postdoctoral Fellow: Chaoyang Fan
Graduate Students: Sungsik Lee, Tianpin Wu, William E. Kaden, Brian Van Devener

Publications resulting from this work:

1. C. Fan, T. Wu, W.E. Kaden, B.V. Devener, and S.L. Anderson, Cluster size effects and effects of surface passivation on hydrazine decomposition on Ir_n/Al_2O_3/NiAl(110). (in preparation).
2. C. Fan, T. Wu, W.E. Kaden, and S.L. Anderson, Cluster size effects on hydrazine decomposition on Ir_n/Al_2O_3/NiAl(110). Surf. Sci., 2006. 600: 461-7.
3. C. Fan, T. Wu, and S.L. Anderson, An inert pulsed hydrazine UHV doser, and N_2H_4 decomposition on a model Ir/Al_2O_3/NiAl(110) catalyst. J. Vac. Sci. Technol., 2006. A 24: 269-74.
4. S. Lee, C. Fan, T. Wu, and S.L. Anderson, Hydrazine Decomposition over Ir_n/Al_2O_3 Model Catalysts Prepared by Size-Selected Cluster Deposition. J. Phys. Chem., 2005. 109: 381-8.
5. M. Aizawa, S. Lee, and S.L. Anderson, Deposition dynamics and chemical properties of size-selected Ir clusters on TiO_2. Surf. Sci., 2003. 542: 253-275.

Statement of Objectives:

Catalytic decomposition of high nitrogen molecules such as hydrazine and mono-methylhydrazine is important in spacecraft thrusters, gas generators and compact power generation units. Typical catalysts are refractory transition metals dispersed on a refractory oxide support, the most common being Shell 405, which is iridium dispersed on a high surface area aluminum oxide support. Lifetime of the catalysts in these systems is limited by several factors, including sintering/agglomeration of the active metal at high operating temperatures, physical damage to the catalyst or support by high pressures developed in cold starts, and chemical changes to the metal or support surfaces that render the catalyst less active.[1-3] New, even more energetic high nitrogen compounds are being developed in various labs for these applications, and these presumably will place even greater demand on the catalyst system.

This research project was aimed at understanding the fundamental chemistry of supported metal nanoparticles, with application to hydrazine decomposition. The immediate goals were to understand the reaction mechanisms and how they change with catalytic particle size and other properties of the model catalysts. The results also bear on questions with broader scientific and technological impacts. In particular, sintering and diffusion of nanoclusters are important issues in the growth and stability of thin film and other nanostructures, with applications to microelectronics, N/MEMS, and nano-scale materials in general.

To carry out the research, the Utah size-selected cluster deposition system was extensively modified, with a new main chamber, and other improvements. A major challenge was to develop a hydrazine and ultra-high vacuum (UHV) compatible gas inlet system. The instrumentation was used in several studies, including one of Ir cluster deposition, structure, and thermal behavior on TiO_2, and three of hydrazine decomposition on Ir clusters grown or deposited on clean, and hydrazine-passivated Al_2O_3 thin films.

Experimental Approach and Instrumentation Developed: The approach is to prepare *model* catalysts by deposition of energy- and size-selected metal clusters on well characterized support surfaces. Unlike conventional catalyst preparation, the cluster size, deposition density, and support defect concentrations (and type) can be varied independently. The instrument combines capabilities for cluster deposition, with *in situ* characterization of the chemical, electronic, and morphological properties of the resulting model catalysts. This instrument is unique in the U.S. with *demonstrated* capabilities for both catalysis and spectroscopic studies of size-selected supported clusters. The main deposition instrument (Fig. 1) allows us to prepare an intense beam of atomically size-selected metal cluster ions, which can be deposited on a well characterized solid support in an ultra-high vacuum (UHV) system equipped with multiple characterization tools. The cluster beamlime[4, 5](Fig. 1, top) can produce clusters using either a 100 Hz pulsed laser vaporization source (shown), or a magnetron sputtering/gas aggregation source, which tends to produce somewhat larger clusters. In either case, the entire size distribution of cluster ions is collected by a series of radio-frequency quadrupole ion guides, and passed through seven differential pumping stages to separate the cluster ions from the large flow of helium gas exiting the source. The beamline includes a bend which allows co-axial injection of the vaporization laser, and also prevents neutral metal vapor from the source from contaminating the deposited sample. Mid-way down the beamline, the clusters pass through a quadrupole mass filter (range: 1 - 4000 amu), allowing us to select the exact size and composition of the cluster beam. Should it prove necessary, it is straightforward to double the mass range by swapping in a smaller diameter quadrupole.

The selected clusters are guided into the UHV deposition/analysis chamber by a final quadrupole (Fig. 1, bottom), where they are deposited through a 2 mm diameter exposure mask, onto the sample. The energy width of the beam is less than 250 meV, allowing deposition at well defined energies down to ~1 eV. Impact energy provides a possible means for influencing both the cluster properties and their tendency to sinter under catalytic conditions. To facilitate the experiments, a new main analysis chamber was built during the first year of the grant period, providing improved control of sample temperature and allowing more streamlined and flexible experimental protocols. Both factors proved critical to the hydrazine experiments.

The model catalyst support surface is typically a single crystal or epitaxial thin film grown on a single crystal. In the new analysis chamber, the sample is mounted on a cryostat, allowing the temperature to be controlled in the temperature range from ~95 K to >1400 K. The sample is suspended from a long-travel manipulator (X-Y-Z translation, axial rotation), which is, in turn, mounted eccentrically on a precision 12" rotating flange system. The combination allows the sample to be positioned and oriented correctly for deposition, or for any of our analysis techniques. In one position of the rotating flange, the manipulator can lower the sample and cryostat out of the bottom of the main chamber, through a triple differentially pumped seal and gate valve, into the separately pumped lower chamber. When the sample is in position in the lower chamber, it is isolated from the main chamber vacuum system, allowing the lower chamber to be used as a high pressure cell (for film growth), or as a load/lock for sample exchange, without degrading the main chamber pressure. Base pressure is typically $<2 \times 10^{-10}$ Torr.

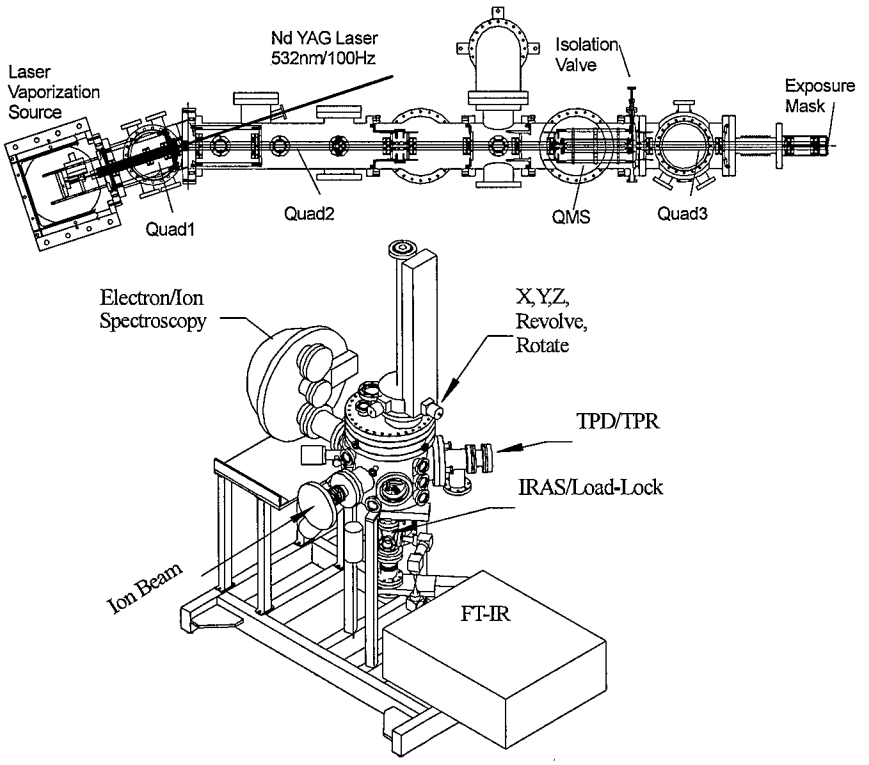

Figure 1. The Utah cluster deposition/chemistry instrument

In addition to deposition, the main chamber has facilities for sample cleaning/annealing, and for growth of epitaxial support films. *In situ* spectroscopic tools include x-ray photoelectron spectroscopy (XPS), Auger electron spectroscopy (AES), and low energy ion scattering spectroscopy (ISS). XPS probes the top 1 - 2 nanometers of the sample, and provides insight into the oxidation state and degree of dispersion of the deposited metal clusters. ISS is sensitive to the identity and relative abundance of each type of atom in the top-most layer of the sample. The combination of XPS and ISS data taken before and after heating, chemical reactions, or other experiments, provides a signature of sintering and other morphology changes. ISS can also be used to detect where (i.e., on which type of surface atom) adsorbates bind when the sample is dosed with reactants. AES provides a fast and sensitive probe of surface composition, with good spatial resolution.

For analysis of adsorption and reactions on the samples, the system has a differentially pumped mass spectrometer, designed to sample only molecules desorbing from the 2 mm cluster spot on the surface. Specifically for working with compounds like hydrazine, we built a new mass spectrometer differential pumping cone that can be cooled to liquid nitrogen temperatures, to trap condensibles desorbing from the sample. We are currently constructing a new cone from aluminum, with the idea that it will be hydrazine-passivated before use, and therefore inert. The mass spectrometry station can be used for temperature-programmed desorption/reaction studies, but we also have constructed two pulsed gas

inlets, that can be used to study chemistry under constant temperature conditions.

One of the challenges of studying reactive species such as hydrazine in UHV, is delivering undecomposed molecules to the surface. Most materials described in the literature as inert to hydrazine,[6] are inert only in the sense that they passivate when exposed to hydrazine. In UHV, a stable passivating layer never forms, therefore catalytic decomposition on inlet surfaces is a serious problem.

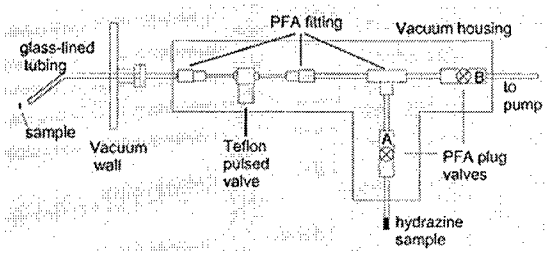

Figure 2. Inert, UHV-compatible pulsed inlet system

To observe catalysis by the small spot of clusters, a truly inert inlet system is essential; furthermore, the system must be leak tight to better than 10^{-10} Torr. After considerable experimentation, the system shown in Fig. 2 was developed. Glass and perfluorinated polymer tubing and plug valves were used to construct the hydrazine reservoir and pump-out system. The hydrazine vapor is metered into the UHV system by a fast micro-solenoid valve, with all working parts constructed from teflon. To minimize hydrazine exposure to the main UHV chamber, the hydrazine is carried to within ~5 mm of the sample by a glass-lined stainless steel dosing tube. Commercial fluoro-polymer valves and fittings are not leak tight for UHV, therefore the entire gas inlet system is enclosed in a small vacuum chamber, rough-pumped to ~100 mTorr. To allow UHV system baking, this inlet vacuum enclosure is cooled during bake-out to prevent the polymer and glass parts from exceeding 70°C. A paper describing the pulsed inlet system, together with some results for hydrazine decomposition on Ir_n/Alumina recently appeared in Journal of Vacuum Science and Technology.[7]

1. Ir_n on TiO_2:

At the beginning of the grant period, we completed a study of Ir clusters on single crystal rutile $TiO_2(110)$. TiO_2 was used for the initial study because it is easy to prepare well characterized, reproducible surfaces, and we had considerable experience working with it. The focus of this initial study was to determine the morphology of the samples prepared by Ir_n^+ deposition, how the morphology might be influenced by deposition energy, and how cluster size and structure relate to chemical behavior. The results are presented in a full paper,[5] and only the most salient points are given here.

The combination of XPS and ISS was used to study the morphology of the clusters, how they bind to the surface, and how adsorbates bind to the clusters. It was found that the clusters make a transition to 3D (multilayer) structures at Ir_5. The ISS shows that the clusters remain intact upon low energy deposition, i.e., they do not shatter or sinter significantly. This conclusion is consistent with calculations of Pala *et al.*[8] showing that Ir-TiO_2 binding is strong and strongly corrugated, even on perfect TiO_2. Binding to oxygen vacancies provides an additional impediment to diffusion. The XPS results also showed that Ir remains in the zero oxidation state under all conditions, including high impact energy, where the Ir becomes implanted into the TiO_2 surface.

One idea for inhibiting catalyst sintering under high temperature conditions is to attach clusters to strongly-interacting defects on the substrate. With energy-controlled deposition, we have the possibility of creating the defects with cluster impact. In this study we were able to show that deposition at energies above 10 eV/atom leads to partial or complete implantation of the Ir_n cluster into the TiO_2 support. Such "embedded" clusters should be quite stable with respect to sintering. Unfortunately, the sintering behavior could not be studied in this system, because the TiO_2 support becomes active at high temperatures, and encapsulates the Ir, even when it is initially deposited on top of the TiO_2 surface.

The Ir_n/TiO_2 samples were further characterized by examining adsorption, exchange, and desorption of $C^{16}O$ and $C^{18}O$, and the effects of thermal cycling on the morphology of the iridium. It was found that small Ir_n on TiO_2 are extremely efficient at adsorbing CO, by a mechanism called substrate-mediated adsorption (SMA), or reverse spillover.[9-11] By exposing the samples to a 0.1 L (1L ≈ 0.25 monolayer equivalents) dose of $C^{16}O$, followed by a 5 L dose of $C^{18}O$, we found something quite interesting. CO delivered to the Ir clusters by SMA results in almost no attenuation of Ir ISS signal, even

though the CO coverage is 60% of the saturation coverage. This implies that SMA-delivered CO binds predominantly into peripheral sites, i.e, CO is associated with the cluster, but not on top of the Ir atoms. On the other hand, when additional $C^{18}O$ is adsorbed in the 5 L exposure, the Ir ISS signal is almost completely attenuated, even though the amount of adsorbed CO only increases by ~40%. The implication is that this additional CO binds atop the Ir clusters, where it attenuates scattering from the underlying Ir.

The existence of distinct "peripheral" and "atop" CO binding sites was verified by temperature-programmed desorption (TPD) measurements, an example of which is shown in Fig. 3. In the lower figure, where the sample was exposed only to 0.1 L of $C^{16}O$, there are two desorption features. The low temperature peak is simply CO weakly bound to defects on the TiO_2 surface, and the high temperature peak is CO bound peripherally to the Ir clusters. The middle data set shows the effect of first dosing with 0.1 L of $C^{16}O$, then with 0.5 L of $C^{18}O$, and the upper data set is for 0.1 L $C^{16}O$ followed by 5.0 L of $C^{18}O$. Note that after exposure to $C^{18}O$, the low temperature peak is converted to $C^{18}O$, indicating efficient CO exchange at the defect sites. In contrast, for the Ir-associated CO binding sites, exchange is not efficient, so that $C^{18}O$ (in atop sites) desorbs at lower temperatures than the $C^{16}O$ in peripheral sites. Similar results are observed for larger clusters, although there is increasing exchange between the peripheral and atop sites during the TPD heating. The ability of ISS to probe adsorbate binding, and the fact that ISS measurements are quick (15 seconds) and very reproducible, is critical to our experiments.

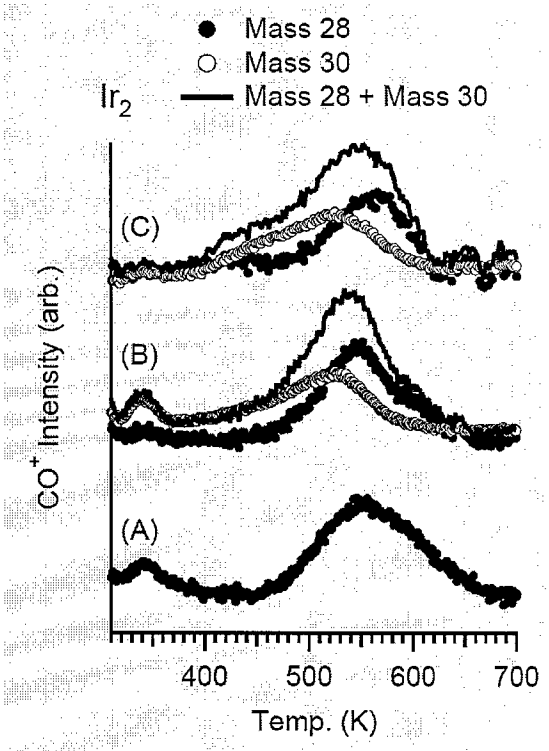

Figure 3. CO TDP from Ir_2/TiO_2: A. 0.1L $C^{16}O$. B. 0.1L $C^{16}O$ + 0.5L $C^{18}O$. C. 0.1L $C^{16}O$ + 5L $C^{18}O$.

2. Hydrazine chemistry on Ir_n

a. Hydrazine/Ir_n/TiO_2:

Having characterized the behavior of Ir_n/TiO_2, we next looked at hydrazine decomposition on this metal/support combination. It turns out that hydrazine decomposes efficiently on TiO_2, itself, making it difficult to work out the effects of the Ir clusters, particularly because we have to keep our Ir coverages below 0.1 ML to minimize cluster-cluster overlap and interaction. TiO_2 also would not be a useful support for a real high temperature catalyst because of its propensity to encapsulate the active metal, and because it tends to lose oxygen at high temperatures, particularly in the presence of oxygen scavengers like hydrazine. We, therefore, did not pursue further work on TiO_2.

b. Hydrazine/Ir_n/Al_2O_3:

Our hydrazine decomposition work has focused on Ir_n/Al_2O_3 – the metal/support combination used in Shell 405 catalyst. Three distinct studies have been completed, in addition to some results reported in the paper describing the inert pulsed inlet.[7] The first, reported in J. Phys. Chem.,[12] reported two independent sets of experiments. One focused on TPD of model catalysts intended to emulate a high Ir loading commercial catalyst, like Shell 405. It turns out that no studies of such catalysts at cryogenic temperatures had been reported. This low temperature behavior is important from a fundamental perspective, but also in understanding thruster cold starts, where a catalyst that has cooled to ambient temperature (which can be cold in space) is exposed to hydrazine. The other component of this initial paper was a continuous flow, steady temperature study, comparing activity of catalysts prepared with size-selected clusters. The results of this paper suggested that interesting size effects might be found in

this system, therefore, we undertook another study, which recently appeared in Surface Science,[13] probing the size dependence in more detail, using both TPD and pulsed reaction mass spectrometry, and taking advantage of the new inert pulsed inlet described in the experimental section. In the course of that study, we discovered that the alumina surface supporting the Ir clusters is somewhat reactive with nascent products of hydrazine decomposition, and that sufficient exposure leads to partial passivation. Therefore, we also studied decomposition of hydrazine on passivated alumina, and this final study is almost completed.

In all these studies, the Al_2O_3 support was prepared by oxidizing single crystal NiAl (110), using the method of Freund and co-workers,[14] which produces a ~5Å thick film with structure similar to that of γ-Al_2O_3 (the typical catalyst support). The NiAl (110) single crystal (Surface Preparation Laboratory) was cleaned by repeated cycles of Ar^+ bombardment followed by annealing at 1220K, then the oxide film was grown using a 1200L O_2 exposure at 550K, with subsequent 950K annealing.[15] XPS and ISS verified that the film was continuous (no exposed Ni) and ~5Å thick. CO TPD was used to verify that there are no strongly-interacting defects on the oxide film, i.e., there is no CO desorption above 95 K (desorption occurs at 310 K on NiAl).[16] . Between each Ir_n^+ deposition experiment, the film, together with all iridium and contaminants, was removed by 1keV Ar^+ sputtering, followed by annealing at 1000K for 15min and at 1220K for 10min, prior to growth of a new oxide film.

Study #1A: High coverage Ir/alumina model catalysts at low temperatures.

Ir was deposited onto freshly-prepared Al_2O_3 films as Ir^+, to a density of 8.0×10^{14} atoms/cm^2, equivalent to 50% of a close-packed Ir monolayer. Under these conditions, Ir clusters form by aggregation of neighboring Ir atoms. Hydrazine (98.5%) was purified with several freeze-thaw cycles using both liquid nitrogen and dry ice/acetone baths, and dosed on the sample from a variable leak valve. Fig.4 shows a series of hydrazine (mass 32) TPD spectra as a function of hydrazine exposure on a clean Al_2O_3/NiAl surface at 93K (i.e, no Ir deposition). For clean Al_2O_3, a negligible fraction of the hydrazine decomposes, thus the spectra are for intact desorption of hydrazine. At low exposures (< 0.2L), hydrazine desorbs in a broad peak centered around ~245K. With increased exposure, the peak narrows and shifts to lower temperature, resulting in a sharp peak at ~185 K for exposures of 1 L and higher, attributed to desorption from a nearly complete monolayer on the surface. For exposures over ~2 L, a new peak appears at 158 K, attributed to desorption from multilayer hydrazine (presumably mostly from a second layer on top of the more strongly bound monolayer). The monolayer packing density of hydrazine on Al_2O_3/NiAl(110) was unknown, and these results allowed us to estimate it at $\sim 6.5 \times 10^{14}$ molecules/cm^2, corresponding to 1.8 L exposure assuming unit sticking. Finally, at much higher exposures, a third peak at a temperature between the multilayer and monolayer peaks is observed. This desorption feature is attributed to crystallization of initially amorphous hydrazine ice.

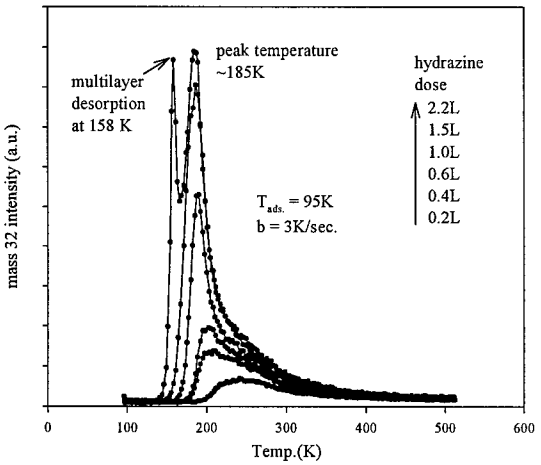

Figure 4. Hydrazine TPD from clean alumina film

Fig. 5 shows desorption spectra of hydrazine and its decomposition products, N_2, NH_3,and H_2, when hydrazine is dosed onto the 0.5ML Ir/alumina sample. After Ir deposition, the samples were exposed to 2.7 L of hydrazine at 93 K, then TPD was done at 3 K/sec heating rate. The relatively high exposure was used so that we could examine behavior of both monolayer and multilayer hydrazine. Raw TPD spectra are shown for mass 32 (hydrazine) and mass 2 (H_2). For H_2, NH_3, and N_2 spectra are shown that have been corrected for contributions from cracking of hydrazine in the mass spectrometer ionizer. (One of the many headaches of studying hydrazine is that ionizer cracking generates the same masses as

ionization of the catalytic breakdown products). As on the clean alumina surface, there is a sharp desorption peak for hydrazine at 164 K, attributed to multilayer (i.e., mostly 2nd layer) desorption. The slightly higher temperature of this peak compared to that for clean Al_2O_3 (158 K) presumably reflects changes in the properties of the underlying monolayer hydrazine from interaction with the deposited Ir. The multilayer peak is useful as an internal standard in correcting for ionizer fragmentation.

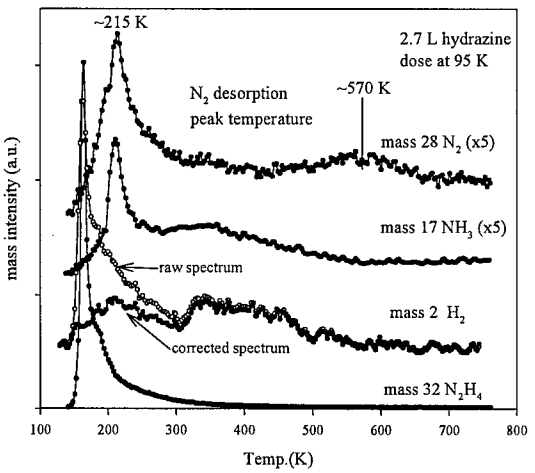

Figure 5. Hydrazine decomposition on Ir/alumina

In contrast to clean alumina, there is no distinct peak corresponding to monolayer hydrazine desorption from Ir/alumina. The mass 32 shoulder at ~185K has about half the intensity of the monolayer desorption peak for clean alumina, and is therefore attributed to intact desorption hydrazine adsorbed on the ~50% of the alumina surface that is Ir-free. The implication is that hydrazine bound to Ir is almost entirely decomposed. N_2 desorption peaks are observed at 215K and 570K. These temperatures are similar to those found for hydrazine/Ir(111)[17] and for hydrazine/polycrystalline rhodium.[18] Ammonia desorption is observed in a sharp peak at 215K and in a broad feature extending from ~ 290 K to ~450 K. The 215 K feature has identical peak temperature and similar width to the analogous low temperature N_2 desorption feature, suggesting that the mechanisms leading to these desorption peaks are coupled. In contrast, the high temperature NH_3 feature appears well below the high temperature N_2 feature. The desorption features we observe for hydrazine/Ir/Al_2O_3 are at somewhat different temperatures than in the two single crystal studies, but the general similarities suggest that the decomposition mechanisms are not drastically different. For H_2, we show both raw and corrected spectra. In the raw spectrum there is a sharp mass 2 peak at 164 K, resulting from ionizer cracking of desorbing multilayer hydrazine. After correcting the spectrum, two mass 2 components remain. The broad peak appearing at ~320K, and extending to ~500 K, appears neither in the mass 32 nor mass 17 spectra. This peak, therefore, is unambiguously attributable to desorption of H_2 decomposition products, presumably generated by recombination of H_{ads}. The corrected mass 2 spectrum also has substantial intensity in the 180 - 300 K range. A bimodal H_2 desorption spectrum was also observed for hydrazine/Rh, and for H_2/Ir(110),[19] but unfortunately H_2 was not monitored in the hydrazine/Ir(111) work.[17]

One issue is whether the desorption features are controlled by N_2 and NH_3 desorption kinetics, or by the kinetics of hydrazine decomposition. The fact that the low temperature N_2 and NH_3 desorption features have identical temperature dependence, suggests that the low temperature is behavior is controlled by hydrazine decomposition. Furthermore, Sawin et al. found that for hydrazine/Ir(111), the low temperature N_2 feature had an extremely sharp angular dependence, indicating some sort of direct reaction, generating N_2 in a strongly repulsive environment.

The high temperature H_2, N_2, and NH_3 features have distinct temperature dependences, and comparison with N_2 and NH_3 TPD experiments on various Ir surfaces, shows that these features result from recombination of various radical species bound to the surface. To check the comparison between Ir/alumina and Ir surfaces, we also measured N_2 TPD following ammonia dosing of our Ir/Al_2O_3 sample at room temperature, i.e., above the temperature where the low temperature ammonia product desorbs. A broad N_2 peak, which must result from recombination, is observed in the temperature range from ~500K to 650K – nearly identical to the high temperature N_2 feature we observe in hydrazine decomposition.

Based on our results and the related studies discussed above, the hydrazine decomposition mechanism seems to break down into distinct low and high temperature parts.[18, 20, 21] As suggested by Sawin et al.,[17] the sharp low temperature N_2 peak is attributed to a direct decomposition reaction on the

surface, generating N_2 that desorbs without accommodating with the surface:

$$N_2H_{4,\,ads} \rightarrow N_2 + 4H_{ads} \qquad T_{peak} \sim 215K$$

The nearly identical desorption feature for NH_3 at low temperatures indicates that the N_2 and NH_3 production mechanisms are coupled. NH_3 might be produced by reaction of H_{ads} with hydrazine:

$$N_2H_{4,\,ads} + 2H_{ads} \rightarrow 2NH_3 \qquad T_{peak} \sim 215K,$$

or by reaction with NH_x(ads):

$$NH_{2,\,ads} + H_{ads} \rightarrow NH_3$$

In addition to the low temperature mechanism, all three products are also observed to desorb in broad, overlapping features in the temperature range from ~280 K to 650 K. Based on the similarities of these desorption features with those observed following dissociative adsorption of NH_3 on various Ir surfaces,[22, 23] the high temperature features are attributed to recombination of NH_x species left on the surface by hydrazine decomposition:[18, 20, 21]

$$N_2H_{4,\,ads} \rightarrow NH_{2,\,ads} + NH_{2,\,ads}$$

$$NH_{2,\,ads} \rightarrow NH_{ads} + H_{ads}$$

$$NH_{ads} \rightarrow N_{ads} + H_{ads}$$

$$NH_{2\,ads} + H_{ads} \rightleftarrows NH_{3\,ads} \rightarrow NH_3 \qquad 280 \sim 450\ K$$

$$H_{ads} + H_{ads} \rightarrow H_2 \qquad 320 \sim 500\ K$$

$$N_{ads} + N_{ads} \rightarrow N_2 \qquad 500 \sim 650\ K$$

Consistent with this sequential mechanism is the observation that once the temperature is high enough to drive recombinative desorption of H_2, the associated reduction in H_{ads} concentration rapidly shuts down NH_3 production, and only N_2 desorption is observed at the highest temperatures.

This mechanism appears to account for hydrazine decomposition on bulk metals and on the high coverage Ir/alumina model catalyst. As shown below, however, the product distribution for small, size-selected Ir_n/alumina is quite different, suggesting that the mechanism is quite strongly dependent on Ir particle size.

XPS was used to probe the chemical state of the adsorbed hydrazine at 95 K, both on clean alumina and on Ir/alumina. For clean alumina, a single N 1s feature at 401.8 eV is observed for a sample containing two layers of hydrazine, indicating that interaction with alumina did not significantly change the chemical environment of the monolayer hydrazine. In contrast, for hydrazine/Ir/alumina, XPS shows two features. One, at 401.8 eV, is attributed to intact hydrazine, both in the multilayer and bound to Ir-free regions of the Al_2O_3. The second peak, at 401.0 eV, is assigned to hydrazine bound strongly to Ir particles, consistent with an earlier study of XPS for hydrazine bound to a variety of metals.[24] No changes in Ir 4f binding energy are observed upon hydrazine adsorption. Ir XPS after the TPD experiment is attenuated by ~30%, consistent with sintering into large particles (average thickness of ~4 layers).

In addition to sintering, catalysts can deactivate if there are changes to the chemical state of the metal or support. Hydrazine monopropellant decomposition occurs under reducing conditions, thus the possibilities are for reduction of the alumina support or formation of nitrides. In this first study, we also used N 1s XPS to examine this issue, and found evidence that a surface nitride compound was forming during TPD. We have pursued this issue, and more detailed information on the nitridation mechanism will be given below.

Study #1B: Continuous hydrazine decomposition over size-selected samples.

Four samples were prepared by deposition of mass selected Ir_n^+ (n = 1, 5, 7, 10) at an energy of 1 eV/atom. To minimize cluster-cluster interactions and sintering in the as-deposited sample, the Ir deposition density was 8.0×10^{13} ***atoms***/cm^2, equivalent to 5% of a close-packed Ir monolayer. Because activity was found to be substantially lower for Ir_1/Al_2O_3, a density of 1.6×10^{14} atoms/cm^2 (10% ML-equivalent) was used. In the results presented here, the sample reactivity has been scaled for this difference in Ir density.

In TPD, hydrazine decomposition occurs at 215 K, with some products desorbing, and some remaining on the surface to desorb recombinatively at higher temperatures. Because we wanted to

examine activity at higher temperatures, we used a continuous flow reaction method, relying on the fact the we have a well defined 2 mm cluster-containing spot, on a 7mm x 7mm Al_2O_3/NiAl substrate. Our differentially pumped mass spectrometer views the sample through an aperture matched to the cluster spot size. It is possible, therefore, to monitor desorption from the Ir-containing spot, or from clean Al_2O_3, simply by translating the sample. After Ir_n^+ deposition, each sample was exposed to a steady state hydrazine pressure of 5 x 10^{-8} Torr at 300 K. This temperature is above the desorption temperature of hydrazine on clean Al_2O_3 and above the low temperature product desorption features on Ir/Al_2O_3. NH_3 product signal was monitored continuously for 60 minutes, during which time the sample was translated repeatedly, to alternately monitor regions of the surface with, and without, Ir_n. The difference in NH_3 signal between the two viewing areas was taken as a measure of activity. The temperature was then increased to 400 K, and the experiment repeated. At a sample temperature of 300 K, we found a substantial increase in NH_3 production when going from the sample prepared with Ir^+ deposition, to the samples prepared with pre-formed clusters. In addition, there is a weak trend to higher activity as the deposited cluster size increases from Ir_5^+ to Ir_{10}^+, although the individual differences are within our estimated uncertainty. This size dependence indicates that the sample properties are influenced by the deposited cluster size, i.e., that sintering or fragmentation of the clusters at room temperature under hydrazine flux does not erase memory of the initial cluster size. The significantly higher activity for Ir_n^+ ($n \geq 5$) compared to Ir^+ suggests, therefore, that hydrazine decomposition activity is size dependent. At 400 K, it appears that the size dependence of the activity is weakened, as would be expected if thermal or adsorbate-induced sample modifications were occurring.

Study #2: Hydrazine TPD from size-selected samples.

This study was similar to that in 1A, described above, except that samples were prepared by deposition of size-selected Ir clusters, rather than by aggregation of non-size-selected clusters on the surface. In addition, we used the improved inlet and mass spectrometer arrangement. The amount of hydrazine decomposition, the product distributions, and the temperature dependence of product evolution all change dramatically with cluster size.

Fig.6 shows a typical TPD scan for a sample prepared by deposition of 0.1 ML-equivalent (1.6 x 10^{14} ***atoms***/cm^2) of Ir_7^+ at 1 eV/atom deposition energy and 100K surface temperature. The sample was exposed to ~3 L of hydrazine, populating both monolayer and multilayer adsorption sites, then ramped in temperature (3K/sec) while monitoring desorption. Multilayer sites were populated for two reasons. First, this desorption peak provides a well defined signature of hydrazine desorption, giving an internal standard for the hydrazine ionizer cracking pattern. In addition, there have been suggestions[17] that second layer hydrazine might be involved in reactions with monolayer hydrazine on Ir(111), and we wanted to look for such decomposition channels. From comparison of experiments on Ir_n/alumina and clean alumina, we find no evidence for any reactions of the second layer hydrazine.

In the figure, the top trace shows N_2H_4 signal v.s. temperature, and the two peaks are assigned as desorption from multilayer (153 K) and monolayer (181 K) sites. The shape is quite similar to what we observe for clean alumina – not surprising given that this sample has only 10% Ir coverage. The next

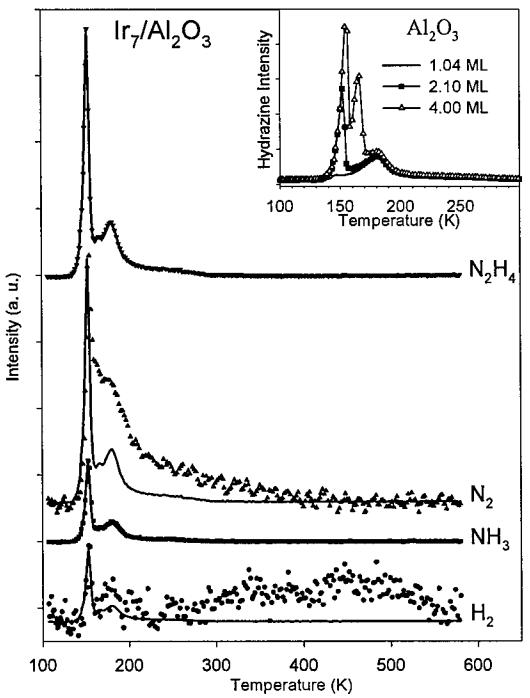

Figure 6. Hydrazine TPD/decomposition on Ir_7/alumina

curve is for N_2, which has contributions from both N_2 produced in catalytic reactions on the surface, and ionizer cracking of hydrazine desorbing from the surface. The sharp peak at 153 K clearly tracks the multilayer hydrazine desorption behavior, and can, therefore be entirely assigned to ionizer cracking. The higher temperature shoulder between 160 and ~400K has contributions from both N_2 production and hydrazine cracking, however, from both the intensity and temperature dependence, it is clear that the dominant contribution is desorption of N_2 from the surface. Because we can measure the ionizer cracking pattern for the multilayer peak, we can easily correct the N_2 signal, and the result is shown in Fig. 7.

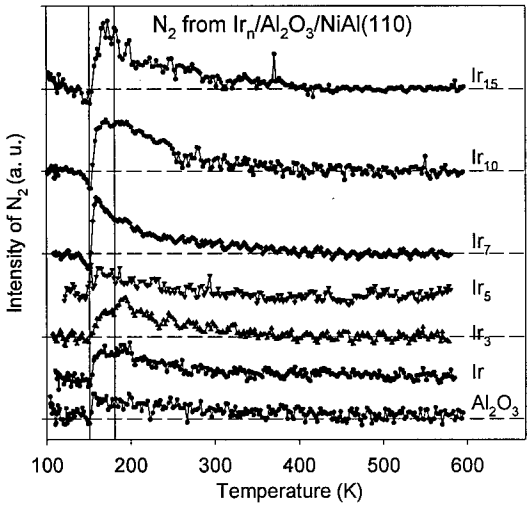

Figure 7. Corrected N_2 TPD signals

The ammonia TPD peak in Fig. 6 tracks the hydrazine temperature dependence quite closely, and after subtracting the ionizer cracking contribution, we find ***no NH_3 production*** within experimental uncertainty. For H_2, the small signal observed at low temperature can be accounted for by hydrazine ionizer cracking, however, there is a broad H_2 desorption feature between ~350K and 550K, similar to the recombinative desorption feature shown in Fig. 5, above. There is relatively high background at mass 2, making accurate measurements of such a broad, weak H_2 desorption feature difficult. We have repeated the measurements using N_2D_4, because there is lower background at mass 4, however, in that case the ammonia product (ND_3) cannot be monitored, because the only commercially available N_2D_4 has ~1% contamination of D_2O, which has the same mass.

There are several points of interest in the TPD results. The most obvious is the observation of no NH_3 production under TPD conditions. This behavior is quite different from what we observed for the larger clusters grown by 0.5 ML Ir^+ deposition, where NH_3 desorbed in two features in this temperature range, with intensity comparable to that of N_2. The difference indicates that the reaction mechanism is quite different on the small clusters in this study. For small clusters, it appears that hydrazine decomposes directly to N_2 gas and H_{ads}, and that H_{ads} recombines to H_2 at high temperatures. These reactions also happen on the larger clusters and bulk metals, however, the small clusters apparently will not support the reactions responsible for NH_3 production and for high temperature N_2 desorption. Taking note of the detailed mechanism discussed above for the high coverage model catalyst, we can infer that reactions such as fission of hydrazine to generate $NH_{x\ ads}$, and reaction of $N_2H_{4\ ads}$ with H_{ads} to generate NH_3, do not occur for these small clusters. Another factor, discussed below, is that the alumina surface can react with adsorbed NH_x products, and this may inhibit desorption of N_2 at high temperatures.

In addition, both the intensity and temperature dependence of the N_2 desorption features (Fig.7) vary with cluster size. For clean alumina, there is a small amount of N_2 production, resulting from hydrazine decomposition at defects in the alumina film. Samples prepared by Ir_n^+ deposition show little additional N_2 production until we reach Ir_7, where the N_2 intensity is substantially increased. This result indicates that small Ir_n ($n < 7$) are inert to hydrazine, but that larger clusters support decomposition to N_2 and H_{ads}, as described above.

A final result of interest is shown in Fig. 8, which compares the ammonia production observed for Ir_{10} and Ir_{15}. Note that for Ir_{10}, there is no net ammonia signal after subtraction of ionizer cracking signal, but that for Ir_{15}, a small ammonia signal is observed. This result indicates that the transition from "small cluster" behavior (no ammonia) to chemistry more typical of large particles or bulk surfaces, has an onset at around Ir_{15}.

Study #3: High coverage pulsed dosing experiments.

As part of the paper describing development of the hydrazine and UHV compatible pulsed doser,[7]

we reported experiments studying constant temperature pulsed hydrazine decomposition on a model catalyst similar to that in study 1A, described above. This sample was prepared by deposition of 0.5 ML of Ir^+, then annealed to 600K to grow clusters. The sample was cooled to 300 K, then exposed to 10 pulses, each amounting to ~1 L hydrazine exposure, while species desorbing from the sample were monitored mass spectrometrically. As in the continuous exposure experiments above, the signals from the Ir-containing spot are compared to background signals measured when the sample is translated so that the mass spectrometer sees only clean alumina. After correcting for ionizer cracking, the pulsed signals are integrated to determine the amount of each product generated. The result is shown in Fig.9, for a sequential set of experiments for $T_{surface}$ ranging from 400 to 600 K. On Ir-free alumina, decomposition is negligible at 400K, but becomes significant at 600 K, with mainly H_2 and N_2 production. For the Ir/alumina spot, decomposition is significant at 400K, producing both NH_3 and N_2. Activity increases with temperature, and at 600K we begin to see substantial H_2 production, in addition of NH_3 and N_2. In a continuous reaction experiment, it would not be clear if the increase in H_2 desorption indicates a change in the hydrazine decomposition branching ratio at 600 K, or simply release of H_{abs} built up on the sample at lower temperatures. In this pulsed experiment, however, it is clear that H_2 desorption tracks the hydrazine pulse, and therefore, H_2 must be coming from decomposition. It is true, however, that at the lower temperatures we are below the peak temperatures observed in the high coverage TPD experiment for recombinative desorption of H_2 and N_2. Therefore, it is reasonable to expect that $NH_{x\ ads}$ and H_{ads} species should build up on the sample, and may react with hydrazine incident on the surface.

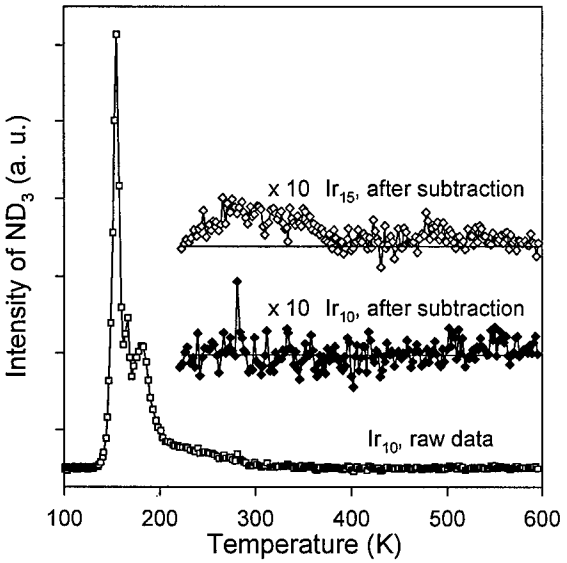

Figure 8. Onset of ammonia production at Ir_{15}

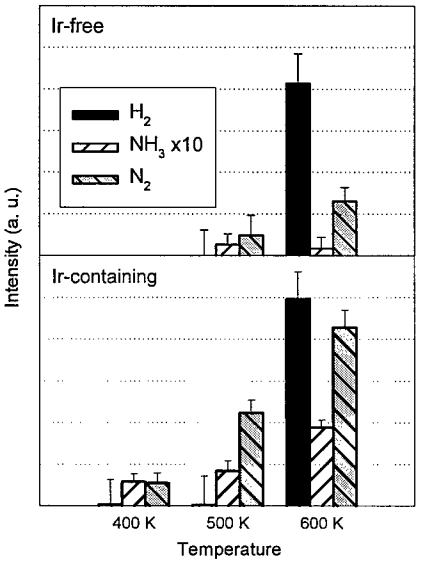

Figure 9. Constant temperature pulsed hydrazine decomposition over Ir/alumina

Support nitridation/passivation:

In both the TPD and pulsed dosing experiments on the high coverage model catalysts, described above, we noticed formation of some nitrogen compound remaining on the surface after the TPD runs. Given the interest in chemical deactivation processes for these catalysts, we carried out an XPS and ISS study to determine the nature of this compound. N 1s XPS shows substantial nitrogen signal after hydrazine exposure, only if Ir is present, indicating that nitridation occurs by reaction with some hydrazine decomposition product. Annealing shows that the nitrogen-containing species is quite stable – we were not able to decompose it thermally. The low N 1s binding energy (~398 eV) observed indicates formation of some strongly bound compound such as a metal nitride or cyanide.[25] Because no carbon is seen in XPS, we infer formation of a nitride or nitride-like compound. Most such compounds are quite refractory, consistent with it not decomposing during annealing. The Ir XPS is unchanged by nitride

formation, indicating that Ir is not involved. The O 1s XPS intensity does not change, showing that N does not displace O, and furthermore, that the nitride does not form onto top of the oxide. This latter point is also clear in ISS, where no N signal is seen. The O 1s binding energy does increase by~0.4 eV, however, indicating that nitride formation changes the oxygen chemical environment, withdrawing electrons from O, on average. Finally, Al XPS also shows a net attenuation by nitride formation, as expected from the increased overlayer thickness, however, there is an increase in the Al^{3+} signal. Therefore, we can conclude that this nitrogen species is a nitride-like compound of some $Al_xO_yN_z$ stoichiometry.

As noted, nitridation is catalyzed by Ir on the surface (with estimated hydrazine-to-nitride conversion efficiency of ~13% for a single TPD run!). Upon closer examination, we discovered that there is also a very small amount of nitride formation that occurs on the Ir-free alumina surface during repeated cycles of hydrazine exposure and heating. This behavior is attributed to hydrazine reaction with defect sites in the alumina film, and it raised the possibility that we might be able to suppress decomposition on the alumina surface by passivation. Using the low temperature N_2 production from monolayer hydrazine as a probe of surface activity, we found that partial passivation is, indeed, possible. In repeated TPD experiments, the N_2 product drops as the surface passivates, eventually reaching steady state where the N_2 intensity, i.e., hydrazine decomposition, is suppressed by a factor of ~3.

Study #4: Hydrazine on Ir clusters on passivated alumina

Fig. 10 shows N_2 production observed in hydrazine TPD from passivated Al_2O_3/NiAl(110), and from samples with 0.1 ML equivalents of various size Ir clusters deposited. Comparison with Fig. 7 shows that N_2 production from the alumina film is largely suppressed (the discontinuities around 160K are an artifact of the ionizer cracking background subtraction). The interesting thing is that in comparison with N_2 from Ir_n on unpassivated alumina, there is generally much less low temperature N_2 production, but N_2 desorption is observed at high temperatures, where none is observed for the unpassivated alumina film. Also in sharp contrast to the unpassivated film, hydrogen desorption is observed in the temperature range between 300 and 400 K for Ir-containing samples (but not for the Ir-free passivated alumina). For both passivated and unpassivated alumina, there is no ammonia production for Ir_n ($n<15$).

There are several possible explanations for the differences in chemistry. It may be that there is significantly different sintering behavior or cluster electronic structure for Ir on passivated, v.s. unpassivated alumina. These issues are being addressed by a combined XPS/ISS study, which allows us to probe morphology and chemical environment of the Ir. In addition, it is clear from the passivation effects on desorption temperature dependence that the alumina surface is involved in the reaction. For the unpassivated alumina, the surface has a significant ability to react with the NH_x intermediates of hydrazine decomposition, and clearly modifies the desorption behavior. In particular, high temperature N_2 desorption is suppressed, presumably because N_{ads} reacts and forms nitrides, rather than recombining and desorbing as N_2. On the other hand, the passivated surface also appears to adsorb NH_x, but reversibly, so that N_2 and hydrogen desorb via recombinative mechanisms at high temperatures. When the XPS/ISS study is completed, we should be able to answer these questions definitively.

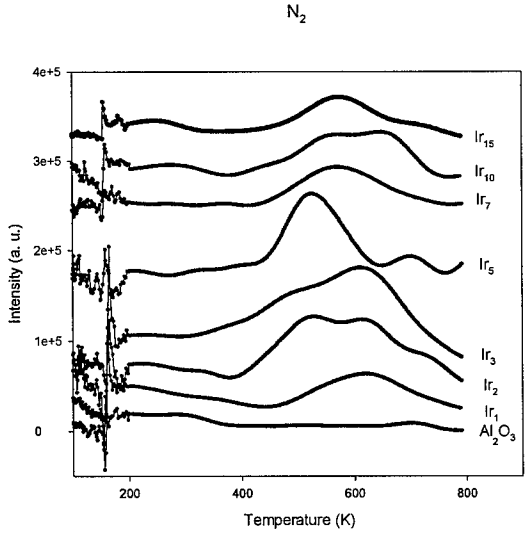

Figure 10. N_2 desorption in hydrazine TPD from Ir_n on passivatedalumina

References

1. S. Balcon, S. Mary, C. Kappenstein, and E. Gengembre, *Monopropellant decomposition catalysts II. Sintering studies on Ir/Al2O3 catalysts, influence of chloride anions.* Appl. Catal., A, 2000. **196**: 179-190.
2. D.L. Emmons, D.D. Huxtable, and D.R. Blevins, *Investigation of a catalytic gas generator for the space shuttle APU.* AIAA Pap., 1974. **74-1107**: 16 pp.
3. H. Greer, *Vacuum startup of reactors for catalytic decomposition of hydrazine.* J. Spacecr. Rockets, 1970. **7**: 522-8.
4. K.J. Boyd, A. Lapicki, M. Aizawa, and S.L. Anderson, *A phase-space-compressing, mass-selecting beamline for hyperthermal, focused ion beam deposition.* Rev. Sci. Instrum., 1998. **69**: 4106-4115.
5. M. Aizawa, S. Lee, and S.L. Anderson, *Deposition dynamics and chemical properties of size-selected Ir clusters on TiO2.* Surf. Sci., 2003. **542**: 253-275.
6. E.W. Schmidt, *Hydrazine and its derivatives.* 2nd ed. 2001, New York: Wiley-Interscience. 2121.
7. C. Fan, T. Wu, and S.L. Anderson, *An inert pulsed hydrazine UHV doser, and N2H4 decomposition on a model Ir/Al2O3/NiAl(110) catalyst.* J. Vac. Sci. Technol., 2006. **A 24**: 269-74.
8. R. Pala, F. Liu, and T. Truong. 2003.
9. J. W C Conner and J.L. Falconer, *Spillover in heterogeneous catalysis.* Chem. Rev., 1995. **95**: 759-788.
10. C.R. Henry, *Catalytic activity of supported nanometer-sized metal clusters.* Appl. Surf. Sci., 2000. **164**: 252-259.
11. M. Boudart, M.A. Vannice, and J.E. Benson., *Adlineation, portholes, and spillover.* Zeitschrift fuer Physikalische Chemie (Muenchen, Germany), 1969. **64**: 171-7.
12. S. Lee, C. Fan, T. Wu, and S.L. Anderson, *Hydrazine Decomposition over Ir_n/Al_2O_3 Model Catalysts Prepared by Size-Selected Cluster Deposition.* J. Phys. Chem., 2005. **109**: 381-8.
13. C. Fan, T. Wu, W.E. Kaden, and S.L. Anderson, *Cluster size effects on hydrazine decomposition on Irn/Al2O3/NiAl(110).* Surf. Sci., 2006. **600**: 461-7.
14. R.M. Jaeger, H. Kuhlenbeck, H.-J. Freund, M. Wuttig, W. Hoffmann, R. Franchy, and H. Ibach, *Formation of a well-ordered aluminium oxide overlayer by oxidation of NiAl.* Surf. Sci., 1991. **259**: 235-252.
15. S. Andersson, P.A. Brühwiler, A. Sandell, M. Frank, J. Libuda, A. Giertz, B. Brena, A.J. Maxwell, M. Bäumer, H.-J. Freund, and N. Mårtensson, *Metal–oxide interaction for metal clusters on a metal-supported thin alumina film.* Surf. Sci., 1999. **442**: L964-L970.
16. C.H. Patterson and T.M. Buck, *The binding site of carbon monoxide on nickel-aluminum(NiAl)(110) determined by low energy ion scattering.* Surf. Sci., 1989. **218**: 431-451.
17. H.H. Sawin and R.P. Merrill, *Angularly resolved temperature-programmed decomposition - nitrogen emission from the decomposition of hydrazine on iridium (111).* J. Chem. Phys., 1980. **73**: 996-998.
18. J. Prasad and J.L. Gland, *Hydrazine decomposition on a clean rhodium surface: A temperature programmed reaction spectroscopy study.* Langmuir, 1991. **7**: 722-726.
19. D.E. Ibbotson, T.S. Wittrig, and W.H. Weinberg, *The chemisorption of hydrogen on the (110) surface of iridium.* J. Chem. Phys., 1980. **72**: 4885-4895.
20. H. Rauscher, K.L. Kostov, and D. Menzel, *Adsorption and decomposition of hydrazine on Ru(001).* Chem. Phys., 1993. **177**: 473-496.
21. R. Dopheide, L. Schröter, and H. Zacharias, *Adsorption and decomposition of hydrazine on Pd(100).* Surf. Sci., 1991. **257**: 86-96.
22. S.A.C. Carabineiro and B.E. Nieuwenhuys, *Selective oxidation of ammonia over Ir(1 1 0).* Surf. Sci., 2002. **505**: 163-170.
23. A.K. Santra, B.K. Min, C.W. Yi, K. Luo, T.V. Choudhary, and D.W. Goodman, *Decomposition of NH3 on Ir(100). A temperature programmed desorption study.* Journal of Physical Chemistry B, 2002. **106**: 340-344.
24. D.J. Alberas, J. Kiss, Z.-M. Liu, and J.M. White, *Surface chemistry of hydrazine on Pt(111).* Surf. Sci., 1992. **278**: 51-61.
25. J.F. Moulder, W.F. Stickle, P.E. Sobol, K.D. Bomben, and J. J. Chastain & R. C. King, eds., *Handbook of X-ray Photoelectron Spectroscopy.* 1995, Eden Prarie, MN: Physical Electronics.